Biosensors and Bioelectronics 138 (2019) 111308

Contents lists available at ScienceDirect

Biosensors and Bioelectronics

journal homepage: www.elsevier.com/locate/bios

A label-free PFP-based photoelectrochemical biosensor for highly sensitive detection of PARP-1 activity

Chenchen Wang[a,1], Ying Li[a,1], Ensheng Xu[a], Qing Zhou[a], Jin Chen[b], Wei Wei[a,*], Yong Liu[c], Songqin Liu[a]

[a] Jiangsu Engineering Laboratory of Smart Carbon-Rich Materials and Device, Jiangsu Province Hi-Tech Key Laboratory for Bio-medical Research, School of Chemistry and Chemical Engineering, Southeast University, Nanjing, 211189, China
[b] The Key Laboratory of Modern Toxicology of Ministry of Education, Center for Global Health, School of Public Health, Nanjing Medical University, Nanjing, 211166, Jiangsu, China
[c] College of Chemistry and Chemical Engineering, Henan University, Kaifeng, 475004, China

ARTICLE INFO

Keywords:
Poly(ADP-Ribose) polymerase-1
Electrostatic interaction
Biosensor
Poly[9,9-bis(6′-N,N,N-trimethylammonium) hexyl]fluorenylene phenylene
Enzyme activity
Detection

ABSTRACT

Poly(ADP-ribose) polymerase-1 (PARP-1), as an original tumor marker, has aroused wide attention in recent years. However, only a few researches have been done for PARP-1 activity detection because PARP-1 is lack of optical or electrochemical property. In this work, a label-free and high-sensitive photoelectrochemical (PEC) biosensor for PARP-1 activity detection based on poly[9,9-bis(6′-N,N,N-trimethylammonium)hexyl]fluorenylene phenylene (PFP) has been designed. To the best of our knowledge, it is the first time that PEC has been used to monitor PARP-1 activity. PARP-1 were activated under the function of activated dsDNA, as a result, branched polymers of ADP-ribose (PAR) with plentiful negative charge were formed in the presence of nicotinamide adenine dinucleotide (NAD^+). Subsequently, positively charged PFP with good photoelectrochemical properties, were absorbed on PAR via electrostatic interaction. High photocurrent was produced under light induction, which was depended on the PARP-1 activity. The biosensor has a wide linear range from 0.01 to 2 U with a detection limit of 0.007 U. The strategy has been applied in breast and ovarian cancer cells to detection PARP-1 activity with approving results, which signifies that it is a promising tool for clinical diagnosis.

1. Introduction

Poly(ADP-ribose) polymerases (PARPs) are a superfamily of signaling enzymes which were discovered in 1963 and composed of 18 members (Sodhi et al., 2010; Ame et al., 2004). Among the superfamily, PARP -1 is the most extensively researched and found member which participates in DNA damage and replication. PARP-1 is a ubiquitous multifunctional nuclear protein involving in DNA break caused by stress of oxidation, radiation stimulation and cytotoxic agents. Furthermore, PARP-1 has been implicated in the process of inflammatory signal transduction and regulation of various proteins expressing in transcription (Szabo et al., 1997; Ullrich et al., 2001). In the process of PARP-1 hyperactivation, nicotinamide adenine dinucleotide (NAD^+) and ATP are the source, after being activated by damaged dsDNA, PARP-1 catalyzes NAD^+ to form linear or branched polymers of ADP-ribose (PAR), which have a lot of negative charges because of luxuriant phosphate groups (Gagne et al., 2006; Meyer-Ficca et al., 2005; Rouleau et al., 2010; Ahmad et al., 2011). Compared to normal cells, PARP-1 is highly expressed in tumor cells, that is why PARP-1 was regarded as an original biomarker for clinical diagnostics particularly for breast and ovarian cancer (Rojo et al., 2012). Therefore, it is urgent to explore more efficient, sensitive and accurate method for detection of PARP-1 activity.

In the past few decades, only a few researches have been constructed for PARP-1 activity detection because PARP-1 is lack of optical, electrochemical or other properties that can be detected easily. The developed techniques included ELISA (Decker et al., 1999), biotin-labeled (Bakondi et al., 2002), radiolabeled (Smith et al., 2005), immunoblotting (Zhang et al., 2013), colorimetry (Xu et al., 2011), fluorescence (Tang et al., 2015; Jiang et al., 2010), electrochemistry (Xu et al., 2016). In our previous work, we have constructed various methods such as UV-vis (Wu et al., 2018b; Liu et al., 2018c), fluorescence (Wu et al., 2018a), electrochemistry (Liu et al., 2018a, 2018b) for PARP-1 detection. Colorimetric method was based on hemin-graphene

* Corresponding author.
E-mail address: weiw@seu.edu.cn (W. Wei).
[1] These authors contributed equally to this work.

https://doi.org/10.1016/j.bios.2019.05.013
Received 18 January 2019; Received in revised form 16 April 2019; Accepted 4 May 2019
Available online 09 May 2019
0956-5663/

nanoparticles. A "turn-off-on" biosensor was constructed based on FRET between MnO_2 nanosheets and PFP. Besides, an electrochemical method based on the hyperbranched-PAR responsive current in AAO membrane was also fabricated and showed superior sensitivity.

Photoelectrochemical (PEC) biosensors have received growing attention in recent years (Dai et al., 2016; Li et al., 2016a,b; Zhao et al., 2015a,b). The PEC biosensor is composed of two relatively independent parts, the PEC active materials (organic/inorganic photoelectric materials) (Ji et al., 2017; Zhang et al., 2016; Zhu et al., 2016; Pang et al., 2018; Han et al., 2018a, 2018b) and the biometric elements (enzymes, antibodies, nucleic acids, etc). The PEC active materials are used to produce the signal of photocurrent and the biometric elements are applied to connect with the transducer (Zhao et al., 2015a,b). Under illumination, the transducers transform the interaction between biometric elements and PEC active materials to photoelectrochemical signals. Such separation of excitation source and detection signal cause higher sensitivity than other detection methods (Shen et al., 2015). In addition, the PEC method is inexpensive and simple, resulting in broad application for detection of biomarkers (such as DNA, enzyme, MicroRNA, etc) (Shi et al., 2016; Liu et al., 2017; Yu et al., 2015; Ma et al., 2016).

Conjugated polymers (CPs) have attracted more attention in biological detection because of their unique optical and electronic properties (Zhu et al., 2012). CPs are composed of π-conjugated backbones and charged side-chains, which make them play a crucial role in bioimaging (Chen et al., 2017), photocatalytic water splitting (Li et al., 2016a,b) and disease therapy (Sun et al., 2015). Apart from the common advantages of other CPs, as a kind of conjugated polymers (CPs), poly[9,9-bis(6′-N,N,N-trimethylammonium)hexyl]fluorenylene phenylene (PFP) also has stable photoelectric property. After light illumination, PFP generates electron-hole pairs, electron acceptors capture electrons migrating along the backbone and then the holes disappear together with photocurrent (Liu et al., 2018).

Inspired by the unique property of PFP and PAR, we constructed a PEC biosensor for PARP-1 activity detection based on the electrostatic attraction of PAR and PFP with high sensitivity and wide detection range. To the best of our knowledge, it is the first time to employ photoelectrochemical method for PARP-1 activity assay. As shown in Fig. S1, the PFP contains abundant positive charge, and poly(ADPribose) (PAR) consists of a large number of ADPs containing abundant phosphate groups which results much more negative charge than dsDNA. Therefore, in the absence of PARP-1, the negatively charged active dsDNA combined only a little PFP, which resulted in weak photocurrent. However, in the presence of PARP-1, hyper-branched PAR were generated under the activation of dsDNA by using NAD^+ as substrate, which subsequently combined much more PFP and led to a higher photocurrent. Thus, a label-free and high-sensitive method to measure PARP-1 activity was constructed.

2. Experiments

2.1. Electrode pretreatment

First, indium tin oxide (ITO) (Ren et al., 2017) slices (25 mm × 5 mm × 1.1 mm) were cleaned ultrasonically with ethanol and water for 3 times in sequence. Then, the cleaned and dried slices were immersed into 1 M NaOH solution for 1 h at room temperature. At last, after being washed and dried again, the hydroxylated slices were immersed into ethanol solution (GR) containing 5% (3-aminopropyl) triethoxysilane (APTES) with gently shaking overnight by shaking table (IKA, KS 260 basic, Germany). Then the obtained ITO electrodes were modified with $–NH_2$ groups (NH_2/ITO).

2.2. Hybridization of active dsDNA

0.5 μM of ssDNA-1 and ssDNA-2 were added into hybridization buffer (see supporting information), followed by heating to 95 °C for 5 min and then cooled to room temperature.

2.3. Detection of PARP-1 activity and its inhibition

First, 10 μL prepared dsDNA were dropped on the reaction parts (5 mm × 5 mm) of NH_2/ITO for 4 h at room temperature (dsDNA/NH_2/ITO). After removing unbound dsDNA, 20 μL 0.1% benzaldehyde solution was dropped on the reaction parts of dsDNA/NH_2/ITO at room temperature overnight. After sucking up excessed benzaldehyde, 10 μL of 500 μM NAD^+ with different concentration of PARP-1 were dropped on the reaction parts for 1.5 h at 37 °C. Finally, the reaction parts were incubated with 10 μL of 20 μM PFP.

A series of inhibitor experiments were performed on 2 U PARP-1 with various concentrations of AG014699. Inhibition efficiency was calculated according to changes of PARP-1 activity. All operations were performed in a humid environment.

2.4. Cell culture

A2780 cells were cultured in Dulbecco's Modified Eagle Medium (DMEM) medium, while MCF-7 and IOSE80 cells were cultured in RPMI-1640 medium. 10% of fetal bovine serum was mixed separately with the above two mediums containing penicillin and streptomycin to support cells survival. Then they were incubated in humid environment with the atmosphere of 5% CO_2 and 95% air at 37 °C.

2.5. Extraction of cytoplasm and nucleus of cells

Both cancer cells (A2780 and MCF-7) and normal cells (IOSE80) were extracted according to the following steps. Firstly, cells were washed by 1 × PBS one time or treated by ethylenediaminetetraacetic acid (EDTA), the obtained cells were centrifuged and supernatant were discarded. After that, the cytoplasmic protein and nuclear extraction reagent were added respectively followed by vigorous shaking. Finally, the obtained mixture was centrifuged at 12000 rpm for 5 min at 4 °C. Supernatants of cytoplasm and nuclei were stored in precooling centrifuge tubes at −80 °C, respectively.

All photoelectric measurements were performed in 10× PBS (pH = 7.4) under the Xe lamp (150 W, Beijing NBeT Co., Ltd.). Electric potential was applied at −0.2 V.

3. Results and discussion

3.1. Principle of the assay

The principle of photoelectrochemical detection of PARP-1 activity was illustrated in Scheme 1. After hydroxylation and amination, the ITO electrodes were modified with dsDNA by Schiff Base reaction and the inactive sites were blocked by benzaldehyde (BzH) (Scheme 1A). In the absence of PARP-1, the negatively charged dsDNA combined with PFP through electrostatic interaction when the positively charged PFP was added, which resulted in weak photocurrent induced by excitation light source. In the presence of PARP-1, it was activated by active dsDNA and catalyzed the broken of glycosylic bond that linked nicotinamide with ribose. The obtained ADP-ribose unites polymerized to hyper branched polymers containing 200 ADP-ribose moieties with abundant phosphate groups, resulting much more negative charges than dsDNA (Xu et al., 2011, 2016; Wang et al., 2014). Therefore, PAR attracted plenty of PFP by electrostatic interaction and led to a higher photocurrent (Scheme 1B). The cathodic photocurrent was strongly depended on the PARP-1 activity, which could be applied to detect PARP-1 activity.

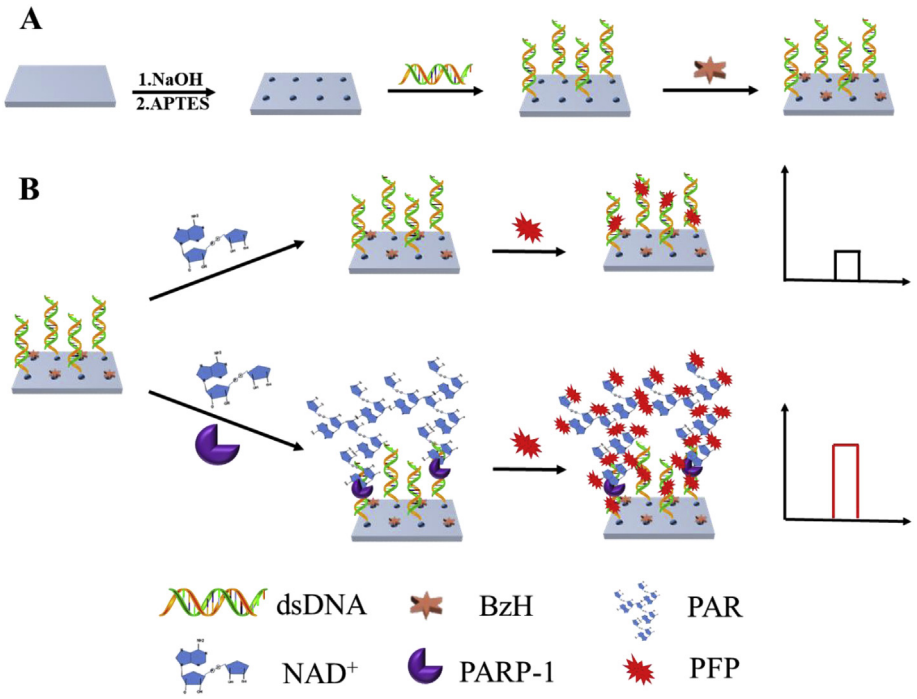

Scheme 1. Schematic illustration of (A) electrode modification process and (B) working mechanism of PEC biosensor for PARP-1 detection using cationic PFP as photocurrent responsive material.

3.2. Feasibility of the PEC biosensor

In this section, the feasibility of the PEC biosensor for PARP-1 activity detection has been discussed. As shown in Fig. 1, the photocurrent of bare ITO (ITO) was almost zero (curve a), after the specific dsDNA were modified (dsDNA/ITO), there was a weak photocurrent because of the negative charge on DNA (curve b). The presence of BzH or 500 μM NAD^+ has no evident effect on the photocurrent (curve c and d). When heated PARP-1 was added, it could not catalyze NAD^+ to form PAR, as a result, the photocurrent remained weak (curve e). However, when activated PARP-1 was added, it catalyzed NAD^+ to generate hyper branched PAR with large negative charges and resulted in high photocurrent (curve f). These experiments proved that the increased photocurrent was induced by PAR catalyzed by PARP-1, so it is reasonable to construct a PEC biosensor for PAPR-1 detection.

3.3. Characterization of the PEC biosensor

The stepwise modification of the PEC biosensor was illustrated in Fig. 2. Cyclic voltammetry (CV) was conducted in 20 mL of 0.1 M KCl containing 5 mM $[Fe(CN)_6]^{3-/4-}$ with a scan rate of 100 mV/s. As shown in Fig. 2A, a pair of reversible redox peak was presented on the bare ITO (curve a). With the successful modification of specific dsDNA and BzH on the surface of ITO, the peak current decreased (curve b and c). When activated PARP-1 catalyzed NAD^+ to produce branched PAR and assembled perfectly, the current peak decreased obviously (curve d), which was mainly ascribed to the electrostatic repulsion between negatively charged PAR and $[Fe(CN)_6]^{3-/4-}$. When positively charged PFP were fabricated, the redox peak decreased further (curve e) because of the dominance of the steric hindrance effect.

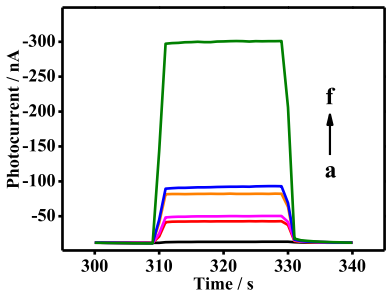

Fig. 1. Photocurrent responses of (a) bare ITO, (b) dsDNA/ITO, (c) NAD^+/dsDNA/ITO, (d) PARP-1/dsDNA/ITO, (e) heated PARP-1/NAD^+/dsDNA/ITO and (f) PARP-1/NAD^+/dsDNA/ITO. The measurement was performed in 10 mL 10× PBS (pH = 7.4) at applied potential of −0.2 V.

Furthermore, electrochemical impedance spectra (EIS) was also performed to illustrate the preparation of the PEC biosensor. As depicted in Fig. 2B, the bare ITO had a low charge transfer resistance (curve a). When negatively charged dsDNA was modified on the surface, the resistance value (R) had a slight increase because of the repulsion between the phosphate and the redox probe (curve b). After the nonconductive BzH were modified on the electrode, they impeded the transfer of $[Fe(CN)_6]^{4-/3-}$ to the electrode, as a result, R increased further (curve c). In the presence of NAD^+ and PARP-1, R increased obviously because of both steric hindrance and bulk charge effect of PAR (curve d). At last, when positively changed PFP adsorbed, R increased further on account of the big steric hindrance effect (curve e). These results indicated that the sensor had been constructed successfully.

3.4. Condition optimization of the PEC biosensor

Four experimental conditions including dsDNA concentration, dsDNA modified time, PAR amplification time and electric potential were optimized to obtain excellent analytical performance. The concentration of dsDNA had a remarkable influence on background signal. As shown in Fig. S3A, background signal increased gradually with the increase of dsDNA concentration from 0.05 to 5 μM, however, the response signal after the addition of PARP-1 was up to maximize at the dsDNA concentration of 0.5 μM. Furthermore, the signal-to-noise ratio of 0.5 μM was the highest because of the steric hindrance effect. According to these results, 0.5 μM was chosen as the most suitable concentration of dsDNA. The modified time of dsDNA exerted a significant effect on the signal response. As illustrated in Fig. S3B, the photocurrent

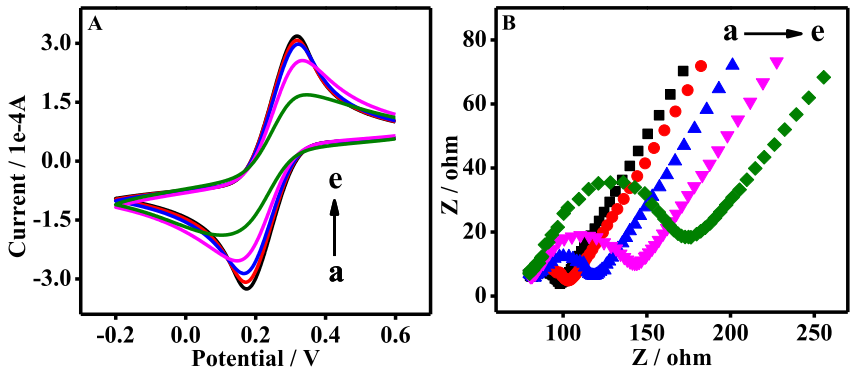

Fig. 2. CV (A) and EIS (B) responses corresponding to (a) bare ITO, (b) dsDNA/ITO, (c) BzH/dsDNA/ITO, (d) PAR/BzH/dsDNA/ITO and (e) PFP/PAR/BzH/dsDNA/ITO. 20 mL 0.1 M KCl containing 5 mM $[Fe(CN)_6]^{3-/4-}$ was performed as detection buffer.

signal rose gradually from 0 to 4 h and then reached a platform. Hence, 4 h was selected as the most appropriate modified time.

PAR amplification time was another crucial factor to affect the photocurrent signal. As shown in Fig. S3C, with the amplification time of PAR increased from 0 to 60 min, the photocurrent signal increased as well and remained the same until 120 min. Therefore, we chose 90 min as the optimal amplification time. Electric potential also played important role in photocurrent detection. As demonstrated in Fig. S3D, the photocurrent intensity increased sharply on changing the applied electric potential from −0.3 to −0.2 V and declined obviously between −0.2 V and 0.2 V. Therefore, −0.2 V was applied for the following research.

3.5. Detection performance of the PEC biosensor

Under the optimal condition, the biosensor performance was evaluated. According to Fig. 3, the photocurrent intensity increased linearly with increment of PARP-1 concentration from 0.01 to 2.0 U. Besides, an excellent linear relationship between PEC signal and PARP-1 concentration was observed in inset. The linear equation for PARP-1 was described as I = - 79.50–106.18 C_{PARP-1} (R^2 = 0.9981), where I and C represented photocurrent intensity and PARP-1 concentration. The detection limit was calculated to be 0.007 U (S/N = 3), which meant the biosensor had a high sensitivity for PARP-1 detection. These results indicated that the PEC biosensor had a wider linear range and comparable sensitivity compared with most reported methods.

Stability and selectivity of the PEC biosensor were studied. As illustrated in Fig. 4A, 12 cycles had been scanned to access the stability of the PEC biosensor, which indicated a satisfying stability of the biosensor. To investigate its selectivity, we chose telomerase, BSA and HRP as interferences. As shown in Fig. 4B, in comparison to PARP-1, weak photocurrent of telomerase, BSA and HRP were observed. In addition, heated PARP-1 produced a similar photocurrent to these interferences. These results manifested that the PEC method had an outstanding selectivity for PARP-1 detection.

3.6. Inhibition efficiency of PARP-1

The inhibition efficiency (%) was calculated as follows:

$$\text{inhibition}\ (\%) = \frac{I_2 - I_3}{I_2 - I_1} \times 100\%$$

where I_1 was the photocurrent of no PARP-1, I_2 was the photocurrent of 2 U PARP-1 and I_3 was the photocurrent of 2 U PARP-1 with different concentration of inhibitor. As depicted in Fig. 5, the inhibitory effect of AG014699 for PARP-1 activity enhanced with the increasing concentration of inhibitor. The IC_{50} of AG014699 was 9.21 nM, indicating that the inhibitor had a perfect inhibition efficiency. And the assay could help to find original and more effective anti-cancer medicine for tumor therapy.

3.7. Detection of PARP-1 in human serum and cancer cells

To certify the PEC biosensor could be applied to detect practical samples, PARP-1 of various concentrations (0.05 U, 0.1 U, 0.4 U, 0.8 U 1.2 U and 1.6 U) were added into standardized human serum diluted with amplification buffer (see supporting information) in 1:10 ratio. The results were shown in Table 1. The recoveries of PARP-1 in human serum were from 97% to 104.8%, indicating the method was accurate. The relative standard deviations were from 0.25% to 4.09%., which indicated that the PEC method has good reproducibility.

Furthermore, human ovarian cancer cells A2780, breast cancer cells MCF-7, and normal ovarian cells IOSE80 were applied to the analysis of PARP-1 activity. As shown in Table 1, the found amount of PARP-1 in A2780 were 0.4243 U in nuclei and 0.1819 U in cytoplasm respectively per 50 cells. Similar to A2780, 0.4028 U in nuclei and 0.2220 U in cytoplasm were found in 50 cells of MCF-7. While for 4000 cells of IOSE80, the content of PARP-1 were 0.0613 U and 0.0385 U found in nuclei and cytoplasm, respectively. In addition, Human PARP ELISA Kit (Jin Yibai Biological Science and Technology Co., Ltd., Nanjing) was also adopted to monitor PARP-1 activity in these cancer cells and the results were close to our proposed method (Table 1). All these results

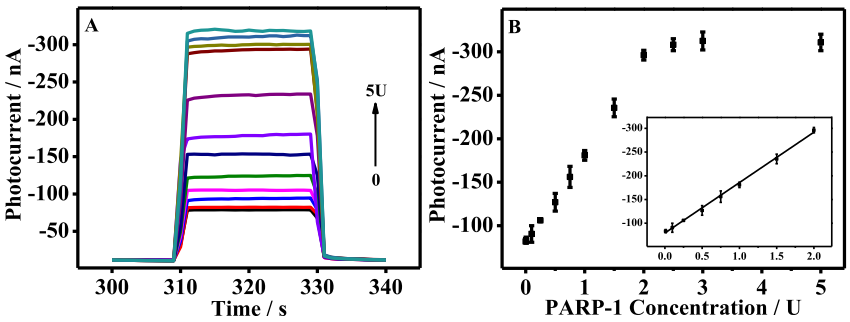

Fig. 3. (A) PEC responses of this biosensor incubated with various PARP-1 concentrations: 0 U, 0.01 U, 0.1 U, 0.25 U, 0.5 U, 0.75 U, 1 U, 1.5 U, 2 U, 2.5 U, 3 U and 5 U. (B) Plot of photocurrent change versus concentration of PARP-1. Insert: the calibration curve for PARP-1 detection. The measurement was performed in 10 mL 10× PBS (pH = 7.4) at applied potential of −0.2 V.

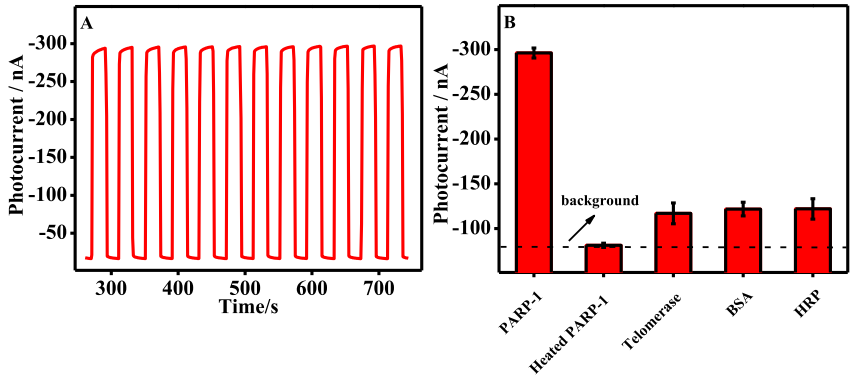

Fig. 4. (A) Stability of this biosensor in the presence of 2 U PARP-1 with continuous off-on-off light for 12 cycles. (B) Selectivity of this biosensor for different targets: PARP-1, heated PARP-1, telomerase, BSA and HRP. The measurement was performed in 10 mL 10× PBS (pH = 7.4) at applied potential of −0.2 V.

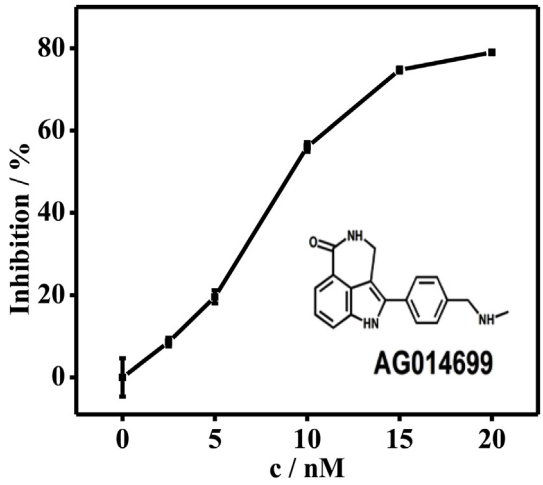

Fig. 5. The PARP-1 inhibitor AG014699 assessment by the proposed PEC method with different concentrations (0, 2.5, 5, 10, 15, 20 nM). The error bar represents the standard deviation of three measurements. The measurement was performed in 10 mL 10× PBS (pH = 7.4) at applied potential of −0.2 V.

Table 1
Detection PARP-1 in human serum and cancer cells and the comparison of them with ELISA method.

Human serum	Added (U)	Found (U)	Recovery (%)	RSD (%, n = 3)
1	0.05	0.049	98	0. 25
2	0.1	0.097	97	0. 42
3	0.4	0.394	98.5	1.46
4	0.8	0.823	102.9	2.16
5	1.2	1.257	104.8	4.09
6	1.6	1.477	98.5	2.99

Cells	Found (U) in Nuclei	Found (U) in Cytoplasm
A2780	0.4243	0.1819
MCF-7	0.4028	0.2220
IOSE80	0.0613	0.0385

ELISA method Cells	Found (U) in Nuclei	Found (U) in Cytoplasm
A2780	0.3091	0.1313
MCF-7	0.2336	0.1358

indicated that the PEC method had good prospect to be used for PARP-1 activity detection in cancer cells.

4. Conclusions

In summary, on basis of the electrostatic interaction of PAR and PFP, a label-free and high sensitivity PEC method with wide linear range was designed. The strategy avoided complex operations, label procedures and expensive instruments. Importantly, no nanomaterial was necessary, which avoided complex preparation of nanomaterial. The linear range was wide enough from 0.01 to 2 U and the detection limit was as low as 0.007 U, which was comparable to most previously reported methods. The method has been successfully applied in human serum, real cancer cells and inhibitor with satisfactory results, therefore the method has a broad potential in clinical diagnosis and cancer drug development. This work proposes a novel label-free enzyme assay and inhibitor evaluation on the basis of PFP, further expanding the applications of these conjugated polymers in bioanalysis.

CRediT authorship contribution statement

Chenchen Wang: Data curation, Writing - original draft. **Ying Li:** Conceptualization. **Ensheng Xu:** Methodology. **Qing Zhou:** Methodology. **Jin Chen:** Writing - review & editing. **Wei Wei:** Funding acquisition, Project administration, Writing - review & editing. **Yong Liu:** Formal analysis, Software. **Songqin Liu:** Supervision.

Acknowledgements

We gratefully appreciate the support from National Natural Science Foundation of China (21775019 and 21635004), Fundamental Research Funds for the Central Universities and A Project Funded by the Priority Academic Program Development of Jiangsu Higher Education Institutions (Grant Nos. 2242018K3DN04), The Open Project of The Key Laboratory of Modern Toxicology of Ministry of Education, Nanjing Medical University (NMUMT201804).

Appendix A. Supplementary data

Supplementary data to this article can be found online at https://doi.org/10.1016/j.bios.2019.05.013.

References

Ahmad, M., Torky, A., Glahn, F., Scheubel, R.J., Foth, H., 2011. Arch. Toxicol. 85, 669–679.
Ame, J.C., Spenlehauer, C., de Murcia, G., 2004. Bioessays 26, 882–893.
Bakondi, E., Bai, P., Szabo, E., Hunyadi, J., Gergely, P., Szabo, C., Virag, L., 2002. J. Histochem. Cytochem. 50, 91–98.
Chen, Z., Yuan, H., Liang, H., 2017. ACS Appl. Mater. Interfaces 9, 9260–9264.

Dai, H., Zhang, S., Hong, Z., Lin, Y., 2016. Anal. Chem. 88, 9532–9538.
Decker, P., Miranda, E.A., de Murcia, G., Muller, S., 1999. Clin. Cancer Res. 5, 1169–1172.
Gagne, J.P., Hendzel, M.J., Droit, A., Poirier, G.G., 2006. Curr. Opin. Cell Biol. 18, 145–151.
Han, Q., Wang, R., Xing, B., Chi, H., Wu, D., Wei, Q., 2018a. Biosens. Bioelectron. 106, 7–13.
Han, Q., Wang, R., Xing, B., Zhang, T., Khan, M.S., Wu, D., Wei, Q., 2018b. Biosens. Bioelectron. 99, 493–499.
Ji, J., Wen, J., Shen, Y., Lv, Y., Chen, Y., Liu, S., Ma, H., Zhang, Y., 2017. J. Am. Chem. Soc. 139, 11698–11701.
Jiang, H., Kim, J.H., Frizzell, K.M., Kraus, W.L., Lin, H., 2010. J. Am. Chem. Soc. 132, 9363–9372.
Li, L., Cai, Z., Wu, Q., Lo, W., Zhang, N., Chen, L., Yu, L., 2016a. J. Am. Chem. Soc. 138, 7681–7686.
Li, R., Yan, R., Bao, J., Tu, W., Dai, Z., 2016b. Chem. Commun. 52, 11799–11802.
Liu, Y., Fan, J., Shangguan, L., Liu, Y., Wei, Y., Wei, W., Liu, S., 2018a. Talanta 180, 127–132.
Liu, Y., Fan, J., Yang, H., Xu, E., Wei, W., Zhang, Y., Liu, S., 2018b. Biosens. Bioelectron. 113, 136–141.
Liu, Y., Xu, X., Yang, H., Xu, E., Wu, S., Wei, W., Chen, J., 2018c. Analyst 143, 2501–2507.
Liu, P., Liu, X., Huo, X., Xu, J., Ju, H., 2017. ACS Appl. Mater. Interfaces 9, 27185–27192.
Liu, S., He, P., Hussain, S., Lu, H., Zhou, X., Lv, F., Liu, L., Dai, Z., Wang, S., 2018. ACS Appl. Mater. Interfaces 10, 6618–6623.
Ma, Z., Xu, F., Qin, Y., Zhao, W., Xu, J., Chen, H., 2016. Anal. Chem. 88, 4183–4187.
Meyer-Ficca, M.L., Meyer, R.G., Jacobson, E.L., Jacobson, M.K., 2005. Int. J. Biochem. Cell Biol. 37, 920–926.
Pang, X., Cui, C., Su, M., Wang, Y., Wei, Q., Tan, W., 2018. Nanomater. Energy 46, 101–109.
Ren, X., Yan, J., Wu, D., Wei, Q., Wan, Y., 2017. ACS Sens. 2, 1267–1271.
Rojo, F., Garcia-Parra, J., Zazo, S., Tusquets, I., Ferrer-Lozano, J., Menendez, S., Eroles, P., Chamizo, C., Servitja, S., Ramirez-Merino, N., Lobo, F., Bellosillo, B., Corominas, J.M., Yelamos, J., Serrano, S., Lluch, A., Rovira, A., Albanell, J., 2012. Ann. Oncol. 23, 1156–1163.
Rouleau, M., Pate, l A., Hendzel, M.J., Kaufmann, S.H., Poirier, G.G., 2010. Nat. Rev. Canc. 10, 293–301.
Shen, Q., Han, L., Fan, G., Zhang, J., Jiang, L., Zhu, J., 2015. Anal. Chem. 87, 4949–4956.
Shi, X., Fan, G., Shen, Q., Zhu, J., 2016. ACS Appl. Mater. Interfaces 8, 35091–35098.
Smith, L.M., Willmore, E., Austin, C.A., Curtin, N.J., 2005. Clin. Cancer Res. 11, 8449–8457.
Sodhi, R.K., Singh, N., Jaggi, A.S., 2010. Vasc. Pharmacol. 53, 77–87.
Sun, H., Yin, B., Ma, H., Yuan, H., Fu, B., Liu, L., 2015. ACS Appl. Mater. Interfaces 7, 25390–25395.
Szabo, C., Lim, L.H.K., Cuzzocrea, S., Getting, S.J., Zingarelli, B., Flower, R.J., Salzman, A.L., Perretti, M., 1997. J. Exp. Med. 186, 1041–1049.
Tang, S., Nie, Z., Li, W., Li, D., Huang, Y., Yao, S., 2015. Chem. Commun. 51, 14389–14392.
Ullrich, O., Diestel, A., Eyupoglu, I.Y., Nitsch, R., 2001. Nat. Cell Biol. 3, 1035–1042.
Wang, Y., Rosner, D., Grzywa, M., Marx, A., 2014. Angew. Chem. Int. Ed. 53, 8159–8162.
Wu, S., Chen, C., Yang, H., Wei, W., Wei, M., Zhang, Y., Liu, S., 2018a. Sensor. Actuator. B Chem. 273, 1047–1053.
Wu, S., Wei, M., Yang, H., Fan, J., Wei, W., Zhang, Y., Liu, S., 2018b. Sensor. Actuator. B Chem. 259, 565–572.
Xu, Y., Liu, L., Wang, Z., Dai, Z., 2016. ACS Appl. Mater. Interfaces 8, 18669–18674.
Xu, Y., Wang, J., Cao, Y., Li, G., 2011. Analyst 136, 2044–2046.
Yu, X., Wang, Y., Chen, X., Wu, K., Chen, D., Ma, M., Huang, Z., Wu, W., Li, C., 2015. Anal. Chem. 87, 4237–4244.
Zhang, Y., Wang, J., Ding, M., Yu, Y., 2013. Nat. Methods 10, 981–987.
Zhang, Y., Zhou, Z., Shen, Y., Zhou, Q., Wang, J., Liu, A., Liu, S., Zhang, Y., 2016. ACS Nano 10, 9036–9043.
Zhao, M., Fan, G., Chen, J., Shi, J., Zhu, J., 2015a. Anal. Chem. 87, 12340–12347.
Zhao, W., Xu, J., Chen, H., 2015b. Chem. Soc. Rev. 44, 729–741.
Zhu, C., Liu, L., Yang, Q., Lv, F., Wang, S., 2012. Chem. Rev. 112, 4687–4735.
Zhu, J., Huo, X., Liu, X., Ju, H., 2016. ACS Appl. Mater. Interfaces 8, 341–349.